Desalination and Water Treatment
www.deswater.com
doi: 10.5004/dwt.2019.23892

152 (2019) 221–233
June

Optimization and modeling of simultaneous adsorption of Cr(VI) and phenol onto Dowex 1X8 ion exchange resin: kinetic and thermodynamic studies

Soumaya Harbi*, Dorra Tabassi, Chiraz Hannachi, Fatma Guesmi, Béchir Hamrouni

Faculty of Sciences of Tunis, University of Tunis El Manar, UR11ES17 Desalination and Water Treatment, 2092 Tunis, Tunisia, Tel./Fax: +216 (71)871282; email: harbi.soumaya@hotmail.com (S. Harbi)

Received 10 April 2018; Accepted 28 January 2019

ABSTRACT

This work investigates the optimization of simultaneous adsorption of Cr(VI) and phenol using Dowex 1X8 ion exchange resin. The morphology of adsorbent was examined under scanning electron microscope and Fourier transform infrared spectroscopy spectrum. Central composite design (CCD) was chosen to examine the effects of pH, adsorbent dose, initial concentrations of Cr(VI) and phenol in the adsorption process. The maximum Cr(VI) adsorption capacity (41.291 mg/g) and the maximum phenol adsorption capacity (5.69 mg/g) were obtained at initial pH (9.6), resin dose (0.621 g), initial Cr(VI) concentration (290 mg/L) and initial phenol concentration (145 mg/g). The CCD data were employed to develop the artificial neural network (ANN). The determination coefficients suggest the reliability of the developed ANN models. The statistical results reveal that CCD has the best performance for prediction compared with ANN. The influence of ionic strength on adsorption process was investigated separately. The increase of ionic strength was slightly decreased the adsorption efficiency of Cr(VI) and facilitates the adsorption of phenol on the surface of adsorbent. The experiments demonstrated that Dowex 1X8 resin had a good potential in the efficient removal of Cr(VI) and phenol from real wastewaters collected from tannery factory. Kinetic models were adjusted to experimental data, and the pseudo-second-order model presented the best fitting. Thermodynamic study depicted that adsorption of Cr(VI) and phenol onto Dowex 1X8 was spontaneous and endothermic.

Keywords: Binary adsorption; Central composite design; Ion exchange resin; Kinetic models

1. Introduction

Heavy metal and organic compounds often coexist in various aqueous ecosystems. They may be toxic and harmful for human health and environment even at low concentrations. Among these pollutants, chromium and phenol are frequently encountered together in wastewaters such as electroplating, leather tanning, textile, paints and pigments [1]. Chromium exists mostly in two oxidation states Cr(III) and Cr(VI). Cr(VI) is 500 times more harmful than the trivalent form [2]. Cr(VI) is most mutagenic and carcinogenic to the living organism and is usually present in the form of chromate CrO_4^{2-} or dichromate $Cr_2O_7^{2-}$ [3–5]. On the other hand, phenol has been reported to be a toxic aromatic organic compound and weak biodegradable pollutant. Exposure of phenol can lead to skin and eyes injuries, headache, vomiting, gastrointestinal disorders, central nervous system depression, lung, kidney, liver and heart damage ultimately leading to death [6]. The permissible limit of Cr(VI) and phenol in industrial discharge has been set as 0.05 and 1 mg/L, respectively [7–10]. In order to comply with these limits, it is essential to find an effective technique to treat these pollutants especially for their simultaneous removal. Adsorption is one of the most attractive approaches for the removal of heavy metals and phenolic compounds due to its

* Corresponding author.

high efficiency, simple and safe treating processes, versatility for different water systems and low cost [11]. Literature reveals that ion exchange resin is a good technique, particularly in water purification, the concentration and removal of metal ions at very low concentrations in chemical process industries [12]. The main advantages of ion exchange resin over other adsorbent are the high chemical and mechanical stability, high selectivity, less sludge volume produced and the ability to meet strict discharge specifications. In this work, Dowex 1X8 anion exchange resin was used to study the simultaneous adsorption of Cr(VI) and phenol from aqueous solution.

There are many ways and procedures to optimize the adsorption process. Traditional single variation method is not a confident method to find the optimum conditions. Nowadays, response surface methodology (RSM) and artificial neural network (ANN) have been widely employed in modeling and optimization processes in environmental studies. RSM is an empirical statistical technique that contributes to the processes of development, improvement and optimization and can simultaneously determine the optimum of several variables with the minimum data by offering appropriate experimental design [13,14]. On the other hand, ANN is inspired from the functioning of biological nervous systems, and proved to be a powerful technique for complex and nonlinear problems with strong ability to learn and predict [15]. Numerous applications of ANN were successfully conducted to solve environmental problems since it is reliable and robust in capturing the non-linear relationships existing between variables (multi-input/output) in complex systems [16]. It is a good alternative to conventional empirical modeling based on polynomial and linear regressions [17].

To the best of our knowledge, there are few studies relating to the adsorption of Cr(VI) and phenol simultaneously. Thus, the present study was devoted to optimize the simultaneous adsorption of Cr(VI) and phenol from aqueous solution using a selective ion exchange resin, Dowex 1X8. At first, the resin was characterized by Fourier transform infrared spectroscopy (FTIR) and scanning electron microscope (SEM). Then, central composite design (CCD) was chosen for the response surface design to examine the effects of initial pH, resin dose, initial concentrations of Cr(VI) and phenol in adsorption process. ANN was developed with the same experimental data of CCD. Subsequently, the results predicted by the RSM and ANN techniques were compared for their predictive capabilities. The applicability of adsorption process for the treatment of wastewater polluted by Cr(VI) and phenol was investigated. Finally, kinetics of adsorption of dyes thermodynamic study was evaluated.

2. Materials

2.1. Adsorbent and chemicals

The ion exchange resin Dowex 1X8 (100–200 mesh) from Sigma–Aldrich (St. Louis, MO, USA) was used in this work as the adsorbent for the adsorption behavior of Cr(VI) and phenol in aqueous solution. It is a strong anionic exchanger with quaternary ammonium functional group and with chloride as the counter ion, which gives it the ability to exchange with other anions. The fresh resin was first washed several times to remove impurities. Then, this resin was dried at 40°C for future use.

All chemical reagents used in the experiments were of high purity analytical grade and purchased from Sigma-Aldrich. The pH values were adjusted with HCl (0.1 mol/L) for acidic level and NaOH (0.1 mol/L) for basic level.

2.2. Simultaneous adsorption studies

Batch adsorption experiments of binary system of phenol–Cr(VI) were performed in 200 mL Erlenmeyer with working volume of 100 mL. The effect of contact time on the simultaneous adsorption of Cr(VI) and phenol was investigated by conducting similar experiments as follows: two solutions of 100 mL containing different concentrations of Cr(VI) and phenol were thoroughly mixed with 0.5 g of adsorbent at contact time of 2–180 min until the achievement of equilibrium.

Then, the effects of operational parameters affecting simultaneous adsorption of Cr(VI) and phenol were studied. The pH varied from 2 to 10, adsorbent dose ranging from 0.5 to 1.5 g, initial Cr(VI) concentration (100–300 mg/L) and initial phenol concentration (50–150 mg/L). Stirring speed was fixed at 120 rpm and temperature was maintained at 298 K in thermostatic bath. The solution was separated from the adsorbent by filtration. The concentration analyses of Cr(VI) and phenol were carried out using UV–Visible spectrophotometer (Tomos V 1100). For Cr(VI), the concentration was determined by reaction with 1,5-diphenylcarbazide as the complexing agent at the wavelength of 540 nm. The concentration of phenol was examined by 4-amino-antipyrine method at 510 nm. The equilibrium adsorption capacities q_e (mg/g) were calculated as follows:

$$q_e = \frac{C_0 - C_e}{m} \times V \tag{1}$$

where C_0 and C_e are the initial and equilibrium concentrations (mg/L) respectively, m is the adsorbent mass (g) and V is the volume of solution (L).

2.3. Experimental design strategy

RSM is an experimental technique invented to find the optimal response within the specified ranges of the factors [18]. RSM proposes various classes such as CCD, Box–Behnken design and three-level factorial design. In this study, CCD was chosen to study the individual and interaction effect of the simultaneous adsorption of Cr(VI) and phenol by using Dowex 1X8 as an adsorbent. The CCD is one of the most common designs used to fit quadratic models between the dependent and the independent variables and was first introduced by Box and Wilson [19]. Generally, CCD consists of $2n$ factorial runs, where n is the number of factors, $2n$ axial runs and n_c center runs [20]. The number of runs N is given by:

$$N = 2^n + 2n + n_c \tag{2}$$

The center points are used to determine the experimental error and the reproducibility of the data [21]. A five level of

CCD with four factors (initial pH, resin dose, initial Cr(VI) concentration and initial phenol concentration) was used to investigate the effects of parameters by STATISTICA 8.0 software and execute the statistical optimization through RSM. The experimental factors and their levels are presented in Table 1.

The adsorption capacities of Cr(VI) and phenol (q_e) were chosen as the responses (y) of the experiments. The mathematical relationship between the independent variables and the response was expressed by the following quadratic equation [22]:

$$y = \beta_0 + \sum_{i=1}^{n}\beta_i X_i + \sum_{i=1}^{n}\sum_{j=1}^{n}\beta_{ij} X_i X_j + \sum_{i=1}^{n}\beta_{ii} X_i^2 \quad (3)$$

where y is the predicted response, X_i and X_j are the independent factors (i and j range from 1 to n). The parameter β_0 is the model constant, β_i, β_{ii} and β_{ij} are the linear, quadratic and second order term coefficients, respectively, and n is the number of independent factors (n = 4 in this study).

The validity, significance and adequacy of the above polynomial equation are estimated by the analysis of variance (ANOVA), particularly by the value of determination coefficient (R^2), Fisher variation ratio (F value) and probability (p-value). After the generation of polynomial model (Eq. (3)), the desirability function (DF) was established to optimize the simultaneous adsorption process. The main advantages of DF are its ability to obtain qualitative and quantitative responses by simple and quick transformation of different responses for one measurement [23]. The experimental responses were converted to DF values, it is in the range of 0 – 1. The 1 indicates the maximum desirability and 0 marks the minimum desirability. Based on the Derringer and Suich [24], the DF equation can be expressed as follows:

$$\begin{aligned} \mathrm{DF}_i &= \left(\frac{U_i - \alpha}{\beta - \alpha}\right)^{w_i}, && \alpha \le U \le \beta \\ \mathrm{DF}_i &= 1, && U > \beta \\ \mathrm{DF}_i &= 0, && U < \alpha \end{aligned} \quad (4)$$

α and β are the lowest and highest obtained values for the response U_i (i = 1, 2, 3…, n) respectively, and w_i is the weight. The individual desirability scores for each predicted response are then combined on a single overall DF, which is calculated to find the optimum set of input variables:

$$\mathrm{DF} = \left[df_1^{v_1} \times df_2^{v_2} \ldots\ldots \times df_n^{v_n}\right]^{1/n}, \qquad 0 \le v_i \le 1 \quad (i = 1, 2 \ldots\ldots n)$$
$$\sum_{i=1}^{n} v_i = 1 \quad (5)$$

where df_i indicates the desirability of the response U_i and v_i represents the importance of responses.

2.4. Artificial neural network approach

ANN is an advanced mathematical modeling procedure which is similar to that of a biological neuron system [25]. In this study, the neural network of MATLAB 7.12.0 (R2011a) mathematical software was used to predict simultaneous adsorption efficiency. Typically, an ANN includes three layers. Input layer had four neurons as follows: initial pH (2–10), resin dose (0.5–1.5 g), initial Cr(VI) concentration (100–300 mg/L) and initial phenol concentration (50–150 mg/L). The adsorption capacities of Cr(VI) and phenol were chosen as the output layer. The hidden layer is an intermediate node between the input and the output layers. Fig. 1 depicts the schematic diagram of the used ANN.

In all analysis, 70%, 15% and 15% of data was applied for training, validation and testing the accuracy of model and prediction, respectively. Training of the ANN was accomplished through the back-propagation algorithm in multilayer perceptions (MLP) which is the most commonly used [26]. Mean squared error (MSE) and determination coefficient (R^2) were used to determine the best structure of three-layer ANN, which were calculated by the following equations:

$$\mathrm{MSE} = \frac{1}{n}\sum_{i=1}^{N}\left(\left|Y_i - Y_{\mathrm{di}}\right|\right)^2 \quad (6)$$

$$R^2 = 1 - \left(\frac{\sum_{i=1}^{N}\left(Y_i - Y_{\mathrm{di}}\right)^2}{\sum_{i=1}^{N}\left(Y_i - Y_m\right)^2}\right) \quad (7)$$

2.5. Real industrial effluent treatment

The efficiency of Dowex 1X8 on the simultaneous adsorption of Cr(VI) and phenol was tested with a real wastewater. We focused mainly on tannery effluents (Tunis, Tunisia) because there are highly concentrated by Cr(VI) and phenol. After filtering, the pH, the salinity and the concentrations of Cr(VI) and phenol of the collected wastewater were determined before and after adsorption experiment.

Table 1
Experimental factors and their levels in the CCD

Factors	Levels			Start point α = 2	
	Low (–1)	Central (0)	High (+1)	–α	+α
(X_1) pH	4	6	8	2	10
(X_2) Resin dose (g)	0.75	1	1.25	0.5	1.5
(X_3) Initial Cr(VI) concentration (mg/L)	150	200	250	100	300
(X_4) Initial phenol concentration (mg/L)	75	100	125	50	150

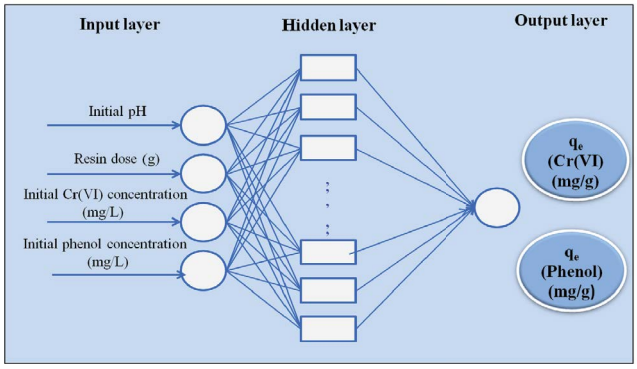

Fig. 1. Topology of ANN.

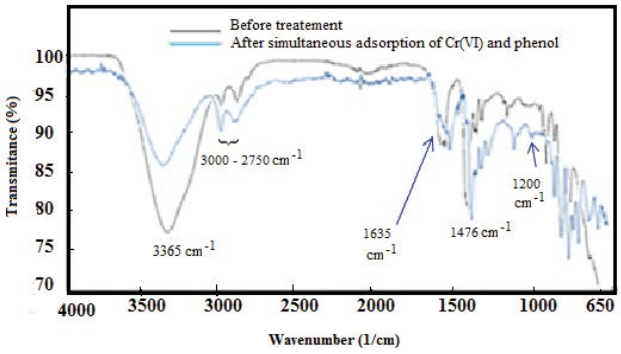

Fig. 2. FTIR of Dowex 1X8.

2.6. Batch kinetic modeling

The kinetic adsorption parameters were investigated using binary solutions. The experiments were carried out by agitating 50 mL of solution at constant concentrations of Cr(VI) and phenol, with 0.5 g of adsorbent, in a constant agitation speed, 298 K and natural pH. The various kinetic models used to describe the adsorption process were analyzed by non-linear regression analysis using OriginPro8.6 software.

Pseudo-first-order model:

$$q_t = q_{cal}\left(1-\exp\left(-K_1 t\right)\right) \quad (8)$$

Pseudo-second-order model:

$$q_t = \frac{K_2 q_{cal}^2 t}{1+K_2 q_{cal} t} \quad (9)$$

where q_e and q_t are the adsorption capacities (mg/g) at equilibrium and at time t, respectively. k_1 (1/min), k_2 (g/mg min) and k_{dif} (mg/g $min^{0.5}$) are the rate constants.

3. Results and discussion

3.1. Characterization of Dowex 1X8

To identify the functional groups available on the surface of Dowex 1X8 before and after the simultaneous adsorption of Cr(VI) and phenol, FTIR studies were carried out with an FTIR spectrophotometer within the range of 650–4,000 cm^{-1} wavenumber. The obtained spectra for the adsorbent are shown in Fig. 2.

As seen from Fig. 2, the strong band at 3,365 cm^{-1} show the presence of stretching vibration of hydroxyl groups [27]. The bands at 3,000–2,750 cm^{-1} were assigned to the C–H stretching mode. The common peaks at 1,476 cm^{-1} were due to C–N vibration of –N+ (CH_3)3Cl− [28]. The changes in the surface functional groups of Dowex 1X8 after adsorption of Cr(VI) and phenol were also confirmed by the changes in the positions of some peaks as well as the appearance of some new peaks. In fact, the strong band at 3,500–3,200 cm^{-1} becomes weak and broad after adsorption. The stretching band of C=C at 1,635 cm^{-1} on Dowex 1X8 before adsorption was shifted to 1,613 cm^{-1} when Cr(VI) and phenol were simultaneously adsorbed. A weaker peak appeared at 1,200 cm^{-1} after the adsorption corresponding to the stretching vibration of C–O in phenol.

The morphology of Dowex 1X8 was further observed by SEM and micrographs are shown in Fig. 3. The image shown in Fig. 3(a) was taken by applying 15 kV voltage with 50 times magnification, while the micrograph shown in Fig. 3(b) was taken at 200 times magnification and the micrograph shown in Fig. 3(c) was taken at 1,000 times magnification for the clear explanation of the surface.

SEM images of Dowex 1X8 particles showed a smooth surface and the particle size were spherical (Figs. 3(a) and (b)). In contrast, the images of Dowex 1X8 particles after adsorption revealed the deposition of foreign materials on the Dowex surface, which could be ascribed to the deposition of the Cr(VI) and phenol (Fig. 3(c)).

3.2. Effect of contact time

In order to verify the equilibrium time of the systems, the effect of contact time on the adsorption of Cr(VI) and phenol by Dowex 1X8 was carried out at different time intervals by selecting two different concentrations of Cr(VI) and phenol. The results are shown in Fig. 4.

As seen in Figs. 4(a) and (b), the equilibrium of simultaneous adsorption of Cr(VI) and phenol was achieved within 50 min even for higher concentration of both compounds and the adsorption capacities (q_e) of Cr(VI) and phenol are not changed significantly with further increase in contact time. This result demonstrates that the adsorption process can be considered very fast. Therefore, all further experiments were carried out for 50 min.

3.3. Central composite design

As mentioned before, the CCD was investigated to explore the influence of four independent variables (initial pH (X_1), resin dose (X_2), Cr(VI) concentration (X_3), phenol concentration (X_4)) at three level (low, central and high) with coded values (–1, 0, +1) and the starting points of +2 and -2 for $+\alpha$ and $-\alpha$, respectively (Table 1). The designed matrix was generated by the statistical software. 30 experiments were achieved and the obtained responses were summarized in Table 2.

3.3.1. Fitting of the model equations and statistical analysis

Based on the data analysis, the quadratic models were suggested as Eqs. (10) and (11):

$$q_e\mathrm{Cr(VI)} = 20.529 - 0.115X_1 - 0.111X_1^2 - 5.852X_2 + 1.618X_2^2 + 5.346X_3 - 0.082X_3^2 + 0.121X_4 - 0.085X_4^2 - 0.011X_1X_2 + 0.01X_1X_3 - 0.087X_1X_4 - 1.379X_2X_3 - 0.049X_2X_4 - 0.093X_3X_4 \quad (10)$$

$$q_e\mathrm{phenol} = 3.441 + 0.616X_1 + 0.016X_1^2 - 0.277X_2 + 0.111X_2^2 + 0.029X_3 + 0.219X_3^2 + 0.793X_4 - 0.055X_4^2 + 0.210X_1X_2 + 0.018X_1X_3 - 0.247X_1X_4 + 0.106X_2X_3 + 0.252X_2X_4 + 0.156X_3X_4 \quad (11)$$

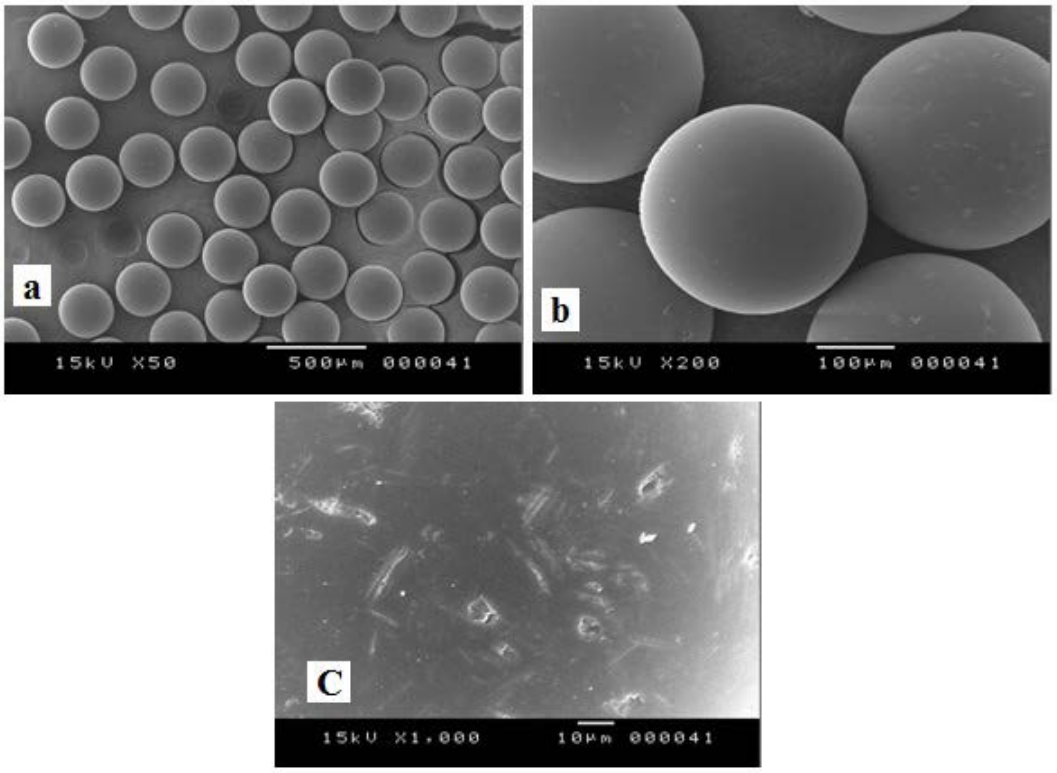

Fig. 3. SEM of Dowex 1X8.

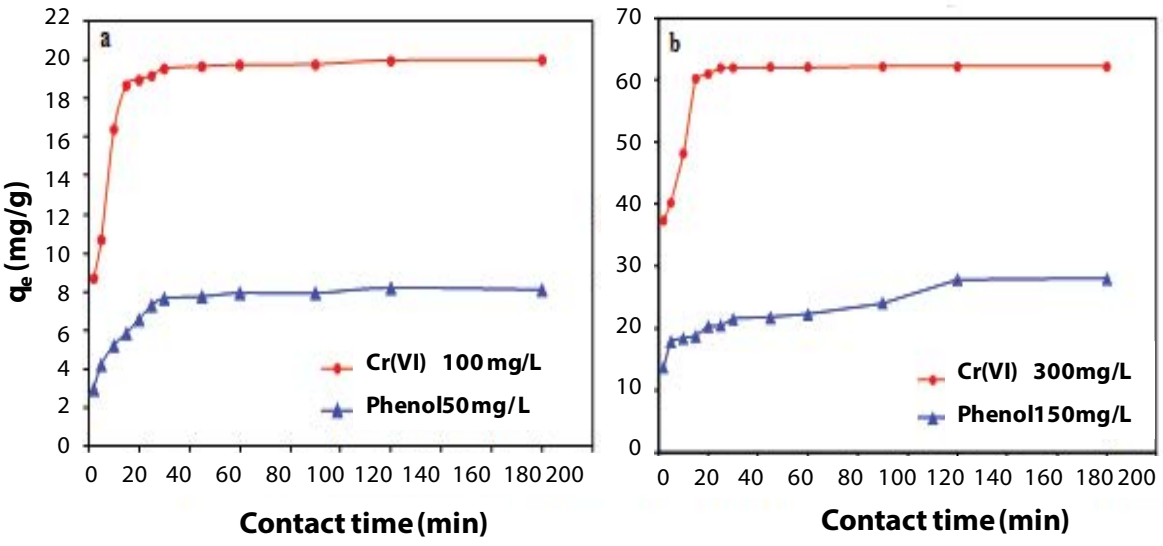

Fig. 4. Effect of contact time onto adsorption of Cr(VI) (a) and phenol (b) by Dowex 1X8 in a multicomponent system.

Table 2
CCD matrix with the observed and predicted responses

Run	X_1	X_2	X_3	X_4	q_e Cr(VI)(mg/g)		q_e phenol(mg/g)	
					Observed	Predicted	Observed	Predicted
1	8	0.75	250	125	33.548	34.342	4.783	4.970
2	4	1.25	250	125	20.154	20.167	3.880	4.035
3	8	0.75	150	75	20.008	20.703	4.244	4.175
4	4	1.25	150	75	12.020	11.934	1.637	1.536
5	6	1	200	100	20.218	20.529	3.450	3.441
6	8	1.25	150	125	12.016	11.989	4.395	4.609
7	8	1.25	250	75	20.139	19.976	3.835	3.644
8	6	1	200	100	20.637	20.529	3.277	3.441
9	4	0.75	250	75	34.156	34.374	2.158	2.402
10	4	0.75	150	125	20.592	21.463	4.217	4.494
11	6	1	200	100	20.628	20.529	3.320	3.441
12	4	1.25	150	125	12.930	12.441	4.080	3.813
13	4	1.25	250	75	20.726	20.033	1.129	1.134
14	4	0.75	150	75	20.026	20.758	3.379	3.229
15	8	1.25	150	75	12.008	11.833	3.237	3.324
16	6	1	200	100	20.643	20.529	3.450	3.441
17	8	0.75	250	75	33.530	34.362	4.090	4.071
18	8	0.75	150	125	20.021	21.057	4.740	4.449
19	8	1.25	250	125	20.147	19.759	5.690	5.555
20	4	0.75	250	100	33.590	34.625	4.148	3.402
21	6	1	200	100	20.654	20.529	3.320	3.441
22	2	1	200	100	20.589	20.315	2.082	2.273
23	6	1	100	100	10.258	9.505	4.209	4.259
24	6	1	200	100	20.655	20.529	3.640	3.441
25	6	1	300	100	31.189	30.891	4.229	4.378
26	6	1	200	150	20.941	20.432	4.886	4.809
27	6	0.5	200	100	41.290	38.709	4.259	4.442
28	6	1.5	200	100	13.771	15.301	3.316	3.334
29	6	1	200	50	20.229	19.945	1.542	1.633
30	10	1	200	100	20.628	19.851	4.730	4.739

The validity of the models was evaluated by the ANOVA and regression coefficients for both responses q_eCr(VI) and $q_e$phenol (Table 3).

According to Table 3, the *F*-values of the quadratic models of q_eCr(VI) and of $q_e$phenol are 74.253 and 23.648, respectively. The higher values of *F* show that the models are significant. Similarly, the fact that *p*-values are less than 0.05 proves the ability of the models and indicates the statistical significance and adequacy at 95% confidence level. Further, considering the lower values of probability (<0.05) and the higher values of *F*, all factors have significant effects in simultaneous adsorption process. Resin dose has the most significant effect on both responses ($p = 0.000$, $F = 710.895$ and 21.614) followed by initial Cr(VI) concentration which has substantial effect on the adsorption capacity of Cr(VI). pH ($F = 106.915$) and initial phenol concentration ($F = 166.486$) have comparatively less significant effect on the response of adsorption capacity of phenol. Sum of squares (SS) of each variable obtained from ANOVA quantifies its importance in the adsorption process and as the value of the SS increases the significance of the corresponding factor also increases. The suitability of the polynomial model equations for Cr(VI) and phenol were also expressed by the determination coefficient R^2 (0.989 and 0.978) and the adjusted R^2 (0.978 and 0.925), respectively, which their values reveal a good predictability of the models. The plots of observed values of adsorption capacities (q_e) vs. those calculated from Eqs. (10) and (11) are given in Figs. 5(a) and (b).

Both figures show a good linear relationship between observed and predicted value. Therefore, it can be concluded that the response surface models developed in this investigation (Eqs. (10) and (11)) were considered to be satisfactory for the prediction of adsorption capacities of Cr(VI) and phenol in the simultaneous adsorption process.

3.3.2. Response surface 3D plots

Response surface plots were developed by considering the significant interactions in the CCD (significant with $p < 0.05$ [Table 3]) to optimize the critical parameters and

Table 3
ANOVA for the quadratic models for simultaneous adsorption of Cr(VI) and phenol

Model term	Cr(VI)					Phenol				
	S.S[a]	d.f[b]	M.S[c]	F-value	*p*-value	S.S	d.f	M.S	F-value	*p*-value
Model	1,506.481	4	376.620	74.253	0.000	25.796	4	6.449	23.648	0.000
X_1	0.317	1	0.317	0.278	0.605	8.972	1	8.972	106.915	0.000
X_2	808.932	1	808.931	710.895	0.000	1.813	1	1.813	21.614	0.000
X_3	675.156	1	675.156	593.332	0.000	0.020	1	0.020	0.249	0.624
X_4	0.329	1	0.329	0.289	0.598	13.972	1	13.972	166.486	0.000
X_1^2	0.340	1	0.340	0.299	0.592	0.007	1	0.007	0.087	0.771
X_2^2	71.604	1	71.604	62.926	0.000	0.341	1	0.341	4.0658	0.062
X_3^2	0.187	1	0.187	0.164	0.690	1.315	1	1.315	15.679	0.001
X_4^2	0.199	1	0.198	0.174	0.681	0.082	1	0.082	0.988	0.335
$X_1 \times X_2$	0.002	1	0.002	0.001	0.967	0.691	1	0.691	8.2393	0.011
$X_1 \times X_3$	0.002	1	0.001	0.001	0.968	0.510	1	0.510	6.0780	0.026
$X_1 \times X_4$	0.110	1	0.110	0.096	0.760	0.873	1	0.873	10.407	0.005
$X_2 \times X_3$	29.712	1	29.712	26.111	0.000	0.175	1	0.175	2.094	0.168
$X_2 \times X_4$	0.035	1	0.034	0.030	0.863	0.908	1	0.908	10.830	0.004
$X_3 \times X_4$	0.124	1	0.123	0.108	0.746	0.347	1	0.347	4.137	0.060
Pure error	0.151	5	0.030	–	–	0.089	5	0.017	–	–
R^2	0.989					0.961				
R^2 adjusted	0.978					0.925				

[a]Sum of squares.
[b]Degree of freedom.
[c]Mean squares.

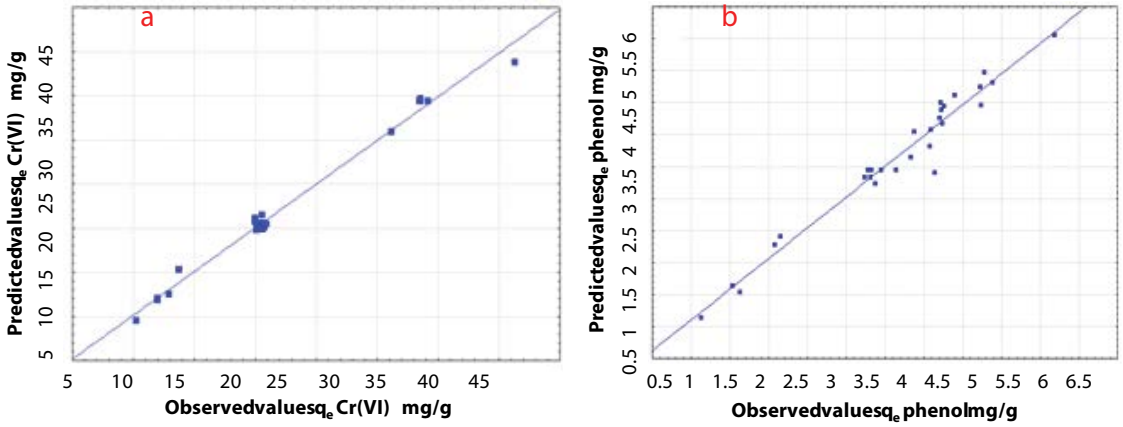

Fig. 5. Observed values vs. the predicted data of simultaneous adsorption of (a) Cr(VI) and (b) phenol.

describe the nature of the responses surface. Figs. 6(a) and (e) represent the interaction plots of adsorption capacity vs. significant variables as two factors at fixed and optimal values of other variables.

The curvatures seen in Figs. 6(a) and (e) confirm the presence of interactions between the variables. Fig. 6(a) shows interactive effect of initial Cr(VI) and resin dose on adsorption capacity of Cr(VI). The adsorption capacity decreases with increasing adsorbent dose due to the reduction in effective surface area and adsorbate/adsorbent ratio [29]. This figure reveals also that the adsorption capacity of Cr(VI) increase with increasing of the initial concentration of Cr(VI) provides increased driving force to overcome all the mass transfer resistance of metal ions between the aqueous and solid phases [30]. The same results were observed with the adsorption capacity of phenol (Figs. 6(d) and (e)).

The combined effect of initial pH and initial phenol concentration on adsorption capacity of phenol is shown in Fig. 6(d). The increase of q_e of phenol with the increasing of initial pH could be explained by considering the presence of ionic and molecular forms of phenols in aqueous solution.

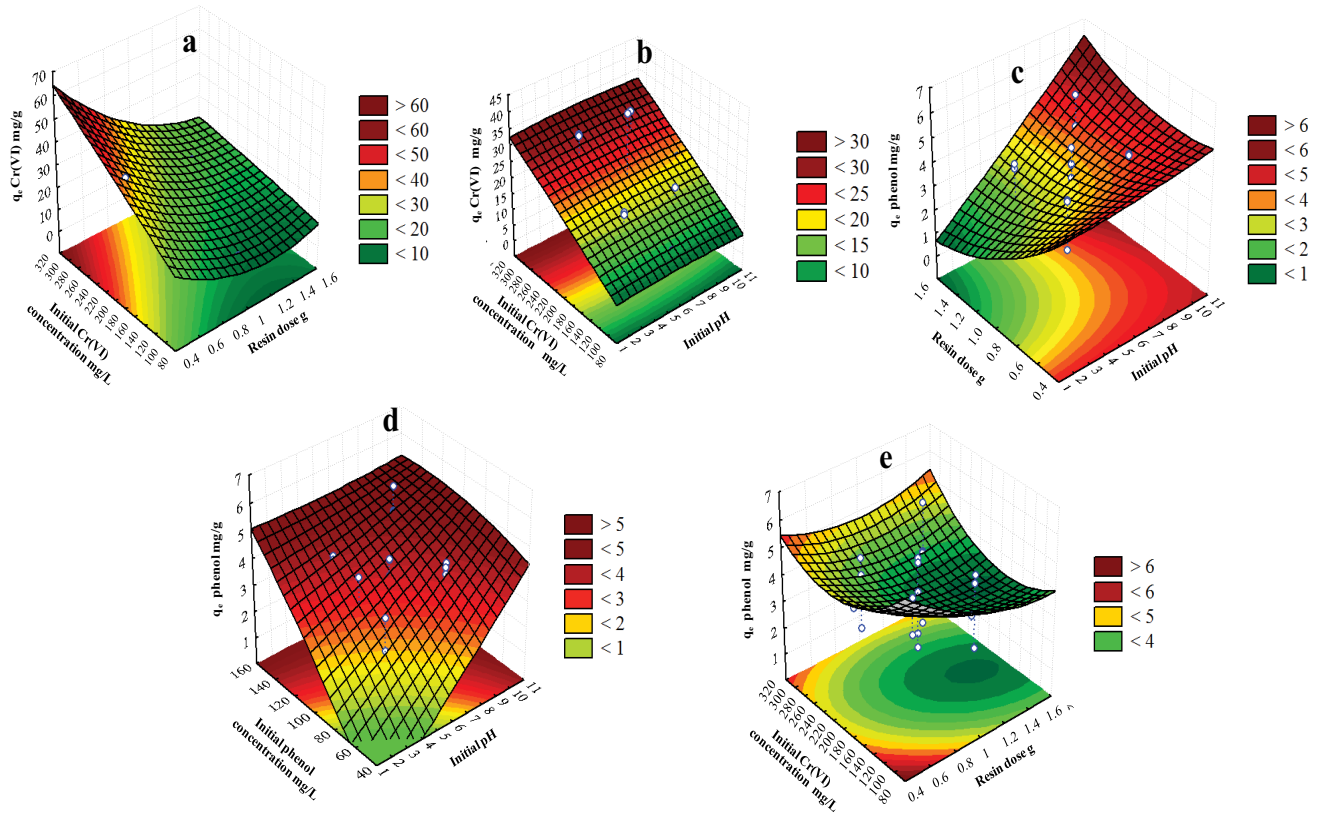

Fig. 6. Response surface plots between (a) initial Cr(VI) concentration and resin dose Cr(VI), (b) initial Cr(VI) concentration and initial pH (phenol), (c) resin dose and initial pH (phenol), (d) initial phenol concentration and initial pH (phenol), (e) initial Cr(VI) concentration and resin dose (phenol).

Phenols act as weak acids in aqueous solution and the dissociation of hydrogen ion from phenols strongly depends on the pH of the solution. In fact, in acidic solutions the molecular form dominates and in alkaline medium the anionic form is the predominant species [31].

3.3.3. Desirability function

The profile for predicted values and DF developed by STATISTICA 8.0 software is used to find the best optimum levels for each variable. Fig. 6 shows the CCD optimization design matrix.

The DF value is in the range of 0 (undesirable) to 1 (very desirable). The CCD optimization design matrix (Fig. 7) indicates that maximum Cr(VI) adsorption capacity (41.291 mg/g and desirability of 1.0) and maximum phenol adsorption capacity (5.69 mg/g with desirability of 1.0) were achieved at following conditions: initial pH (9.6), resin dose (0.621 g), initial Cr(VI) concentration (290 mg/L) and initial phenol concentration (145 mg/g).

3.4. ANN development

ANN was used for modeling the adsorption data obtained by CCD. The best structure of ANN model necessitates the optimum number of neurons in the hidden layer which gives the minimum MSE and the maximum of R^2. Tables 4 and 5 represent the correlation among the number of neurons in hidden layer, MSE and R^2 for both compounds.

From Table 4, the application of 10 neurons in the hidden layer leads to achievement of R^2 and MSE values of 0.999 and 0.005, respectively, for prediction of Cr(VI) adsorption capacity. ANN model with four hidden neurons permits to obtain the best structure with 0.998 and 0.003 of R^2 and MSE, respectively, to predict the adsorption capacity of phenol (Table 5). Therefore, the ANN models, with 10 hidden neurons in the hidden layer for prediction of Cr(VI) adsorption and with four hidden neurons for prediction of phenol adsorption, were used in the following. The regression analyses were used to find the relation between observed data and predicted values using ANN (Fig. 8).

As it can be seen from Fig. 8, the determination coefficients suggest the reliability of the developed ANN models.

3.5. Comparison of CCD and ANN models

At this stage, comparison of CCD and ANN models are needed to validate and test the extrapolative capability of both models. The observed and predicted values by CCD and ANN are presented in Fig. 9.

The performance of the constructed ANN and CCD models was also statistically measured by the root mean

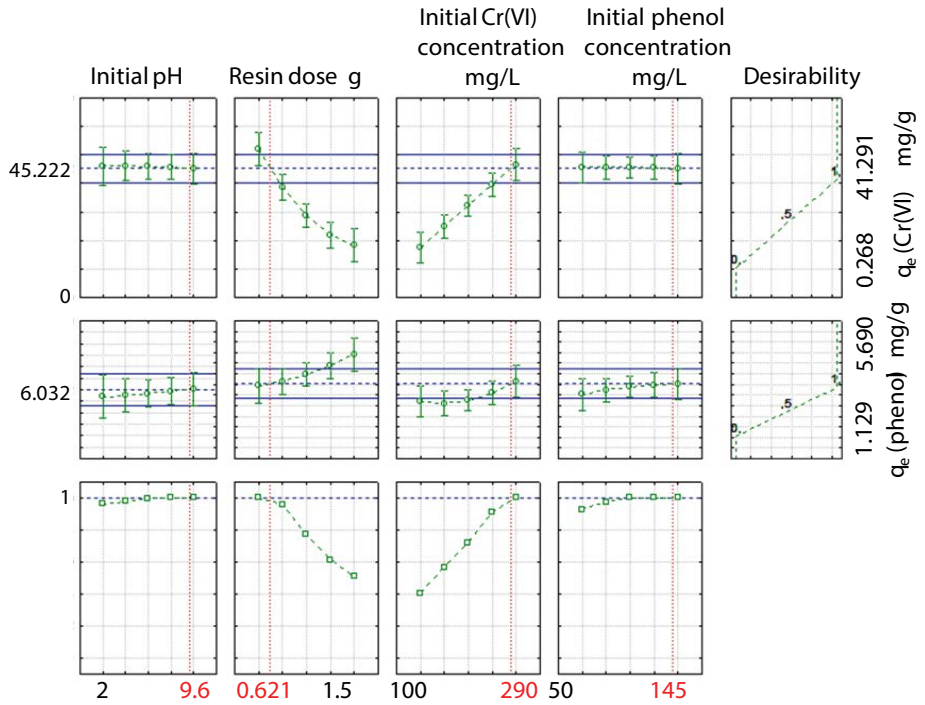

Fig. 7. Profile of desirability function.

Table 4
Comparison of 25 neurons in the hidden layer for Cr(VI) adsorption efficiency by ANN model using back-propagation algorithm in multilayer perceptions (MLP)

Number of neurons	MSE	R^2	Number of neurons	MSE	R^2
1	4.844	0.975	11	0.143	0.998
2	1.870	0.982	12	0.006	0.999
4	2.533	0.983	15	0.009	0.999
6	3.329	0.970	20	0.034	0.999
8	4.112	0.973	25	19.157	0.694
9	0.007	0.999	–	–	–
10	0.005	0.999	–	–	–

Table 5
Comparison of 25 neurons in the hidden layer for phenol adsorption efficiency by ANN model development with back-propagation algorithm in multilayer perceptions (MLP)

Number of neurons	MSE	R^2	Number of neurons	MSE	R^2
1	0.159	0.915	11	0.004	0.997
2	0.155	0.897	12	0.016	0.995
4	0.003	0.998	15	0.115	0.934
6	0.166	0.931	20	0.217	0.913
7	0.044	0.982	25	0.022	0.994
9	0.171	0.957	–	–	–
10	0.009	0.997	–	–	–

squared error (RMSE) and absolute average deviation (AAD) as follows:

$$\mathrm{RMSE} = \left(\frac{1}{N}\sum_{i=1}^{N}\left(Y_i - Y_{\mathrm{di}}\right)^2\right)^{1/2} \tag{12}$$

$$\mathrm{ADD} = \left(\frac{1}{N}\sum_{i=1}^{N}\left(\frac{Y_i - Y_{\mathrm{di}}}{Y_{\mathrm{di}}}\right)\right)\times 100 \tag{13}$$

where N is the number of experimental runs, Y_i is the predicted value and Y_{di} is the observed value.

The statistical comparison of two models is presented in Table 6.

It was evident that the CCD and ANN models were in strong agreement with the experimental results. As it can be seen from Fig. 8, the prediction data lie closer to the line. However, the predictive capability of CCD models was higher than that ANN models. This is confirmed by the values of RMSE and AAD% (Table 6) which are less for CCD than for ANN for both pollutants. Both models have their own interest. CCD has the advantage of showing the interaction effect between independent parameters and their interactions on response as compared with ANN. On the other side, ANN model is very flexible and does not require any standard experimental to build the model [32,34].

3.6. Evaluation of simultaneous adsorption in the presence of various electrolytes in different concentrations

Since the presence of salts in wastewater may greatly affect the potential of adsorption of Cr(VI) and phenol, the

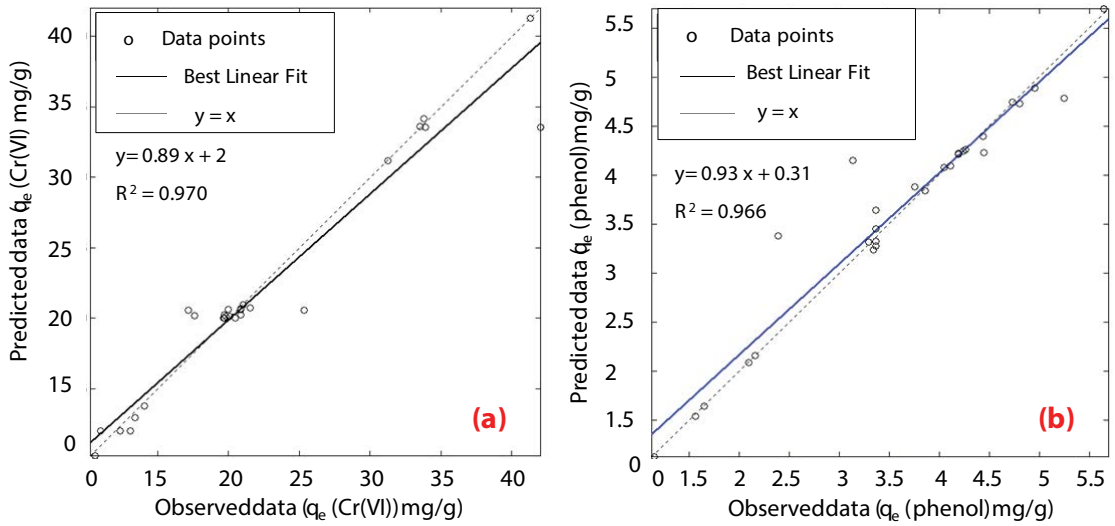

Fig. 8. Comparison of the observed data with those predicted by the ANN model of (a) Cr(VI) and (b) phenol.

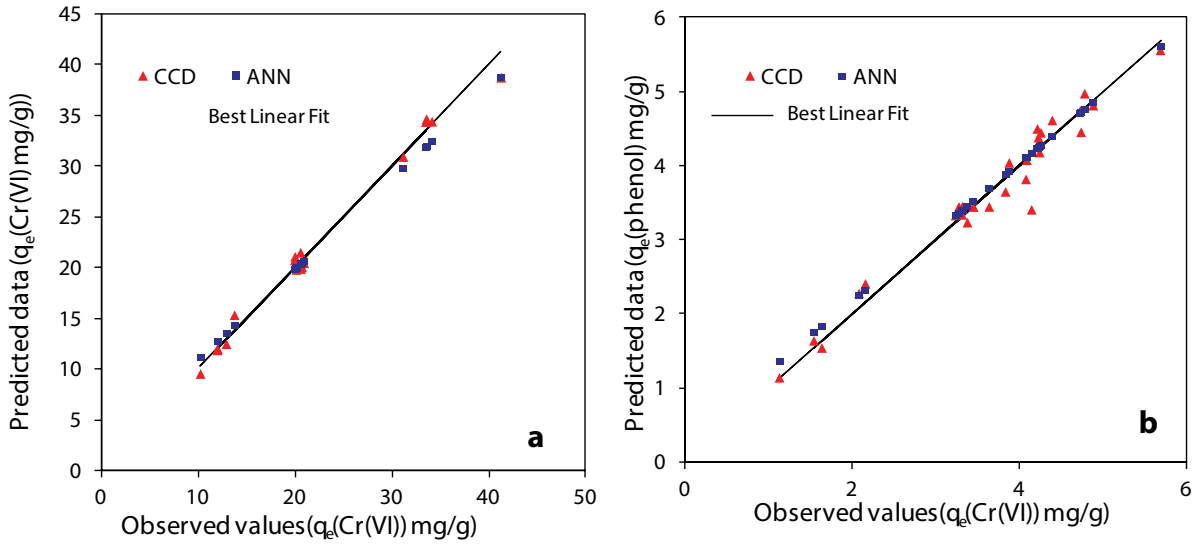

Fig. 9. Comparison of the observed and predicted results via ANN and CCD in simultaneous adsorption of (a) Cr(VI) and (b) phenol.

Table 6
Comparative statistical analysis of CCD and ANN

Parameters	Cr(VI)		Phenol	
	CCD	ANN	CCD	ANN
RMSE	0.284	0.399	0.020	0.040
AAD %	0.023	0.642	0.420	2.741

influence of ionic strength on adsorption process was studied. Fig. 10 shows the effect of various concentrations (10–3, 10–2, 10–1 mol/L) of electrolytes on the adsorption capacities of Cr(VI) and phenol.

The adsorption efficiency of Cr(VI) was slightly decreased with the increase of ionic strength (Fig. 10(a)). The anions also play a moderate role in the ion adsorption process. The Na_2SO_4 salt exercises more inhibitor effect in Cr(VI) adsorption compared with the NaCl, $NaNO_3$,$CaCl_2$ and KCl salts. Indeed, the sulfate ions have a greater competition through enhanced electrostatic interaction in removal of metal among all competing anions present in water [33,34]. Meanwhile, it is different for phenol adsorption. Increasing the ionic strength from 0.001 to 0.1 mol/L led to a significant increase in phenol adsorption. The presence of electrolytes in the solution decreases the solubility of phenol in aqueous solution and shows an effect known as salting-out in the literature [35]. It was reported that the salting-out effect at higher ionic strength has the potential to affect the adsorption process by decreasing the solubility of a non-electrolyte in water [36,37]. Consequently, the increase of ionic strength in aqueous solutions facilitates the adsorption of phenol on the surface of adsorbent. Similar results for adsorption of phenol with other contaminants by other adsorbents were observed by other researchers [11].

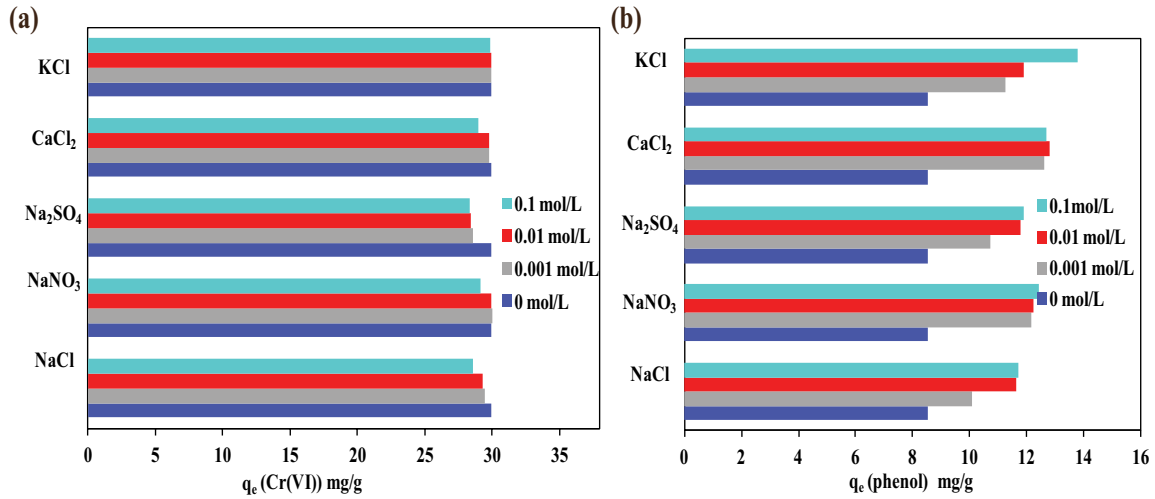

Fig. 10. Effect of ionic strength in simultaneous adsorption of (a) Cr(VI) and (b) phenol.

3.7. Treatment of real wastewater containing Cr(VI) and phenol

The utility of simultaneous adsorption of Cr(VI) and phenol by Dowex 1X8 was demonstrated by treating it with real wastewater obtained from tannery factory. The optimum conditions obtained from CCD (pH: 9.6, resin dose: 0.621 g) were applied to effluent solution. Table 7 shows the characteristics of the sample before and after adsorption process.

The results depict that the residual concentrations of Cr(VI) and phenol after treatment were 70.94 and 65.63 mg/L, respectively. The effect of ionic strength is weak. This test shows that Dowex 1X8 can be successfully used for the removal of Cr(VI) and phenol from industrial wastewater at short equilibrium time.

3.8. Kinetic study

The experimental data for the simultaneous adsorption of Cr(VI) and phenol were applied to the pseudo-first-order and pseudo-second-order kinetic model. The results were verified through the correlation coefficients (R^2) and the Chi-square test χ^2. The value of parameters of kinetic model for Cr(VI) and phenol is depicted in Table 8.

In both the cases, the kinetic data are well agreed with the pseudo-second-order model which is confirmed by the higher value of correlation coefficient R^2 ($R^2 > 0.99$ for Cr(VI) and phenol) and the lower values of χ^2.

3.9. Thermodynamic study

The thermodynamic behaviors for adsorption of Cr(VI) and phenol on Dowex 1X8 were further investigated. The thermodynamic parameters such standard enthalpy change ΔH_T^o, standard free energy ΔG_T^o and standard entropy change ΔS_T^o were evaluated using the following equations:

$$\Delta G_T^o = -RT\ln K \tag{14}$$

$$\Delta G_T^o = \Delta H_T^o - T\Delta S_T^o \tag{15}$$

where R is the universal gas constant (J/mol K), T is temperature (Kelvin) and K is the equilibrium constant calculated as:

$$K = \frac{C_{Ae}}{C_e} \tag{16}$$

where C_{Ae} is the equilibrium concentration (mg/L) of the Cr(VI) ion on the resin and C_e is the equilibrium concentration (mg/L) in the solution.

All the calculated thermodynamic parameters are presented in Table 9.

For the simultaneous adsorption of Cr(VI) and phenol on Dowex, the obtained ΔH_0 values were positive, which indicated the endothermic nature of both component adsorption onto ion exchange resin. The change in entropy was positive,

Table 7
Characteristics of the tannery wastewater before and after adsorption process

Parameters	Values		Adsorption capacity (mg/g)	
	Before treatment	After treatment	Observed	Predicted
Cr(VI) (mg/L)	283.76	70.94	34.27	34.13
Phenol (mg/L)	99.91	65.63	5.52	5.44
TDS (g/L)	6.50	6.34		
pH	12.3	9.1		

Table 8
Kinetic parameters for the simultaneous adsorption of Cr(VI) and phenol by Dowex 1X8 at Θ = 298 K Cr(VI), 50 mg/L of Cr(VI) and 100 mg/L of phenol

Model	Parameters	Compound	
		Cr(VI)	Phenol
Pseudo-first-order model	K_1 (1/min)	0.192	0.123
	q_{cal} (mg/g)	19.613	7.823
	R^2	0.942	0.900
	χ^2	0.849	0.326
Pseudo-second-order model	K_2 (g/mg min)	0.015	0.023
	q_e (mg/g)	20.970	8.477
	R^2	0.942	0.987
	χ^2	0.723	0.104

Table 9
Thermodynamic parameters of Cr(VI) and phenol adsorbed on Dowex 1X8

Component	ΔH_0 (kJ/mol)	ΔS_0 (kJ/mol)	Temperature (K)	ΔG_0 (kJ/mol)
Cr(VI)	49.747	0.210	283	–9,698
			298	–13,005
			313	–15,994
Phenol	7.767	0.027	283	–0,119
			298	–0,419
			313	–0,619

indicating the entropy of the system increased during the adsorption. The negative values of ΔG_0 demonstrated that the adsorption process on Dowex 1X8 was a spontaneous process.

4. Conclusion

In this work, response surface methodology combined with central composite design was used to develop mathematical models and optimize the simultaneous adsorption of Cr(VI) and phenol by strong anionic resin Dowex 1X8. The resin was characterized by the FTIR analysis and SEM. pH, resin dose, initial Cr(VI) concentration and initial phenol concentration were selected as independent factors and the adsorption capacity was considered as response. ANOVA study shows the significance of generated models and depicts that resin dose has the most significant effect on both responses followed by initial Cr(VI) concentration which has substantial effect on the adsorption capacity of Cr(VI). pH and initial phenol concentration have comparatively less significant effect on the response of adsorption capacity of phenol. The optimum conditions were found as initial pH (9.6), resin dose (0.621 g), initial Cr(VI) concentration (290 mg/L) and initial phenol concentration (145 mg/g). The data obtained from CCD were used to model ANN. ANN models using back-propagation algorithms for four independent variables were developed to predict the adsorption capacities of Cr(VI) and phenol. RSM and ANN methodologies were statistically compared. The ionic strength does not affect significantly the adsorption process and the adsorbent was successfully used in simultaneous adsorption of Cr(VI) and phenol from tannery wastewater.

The kinetics of Cr(VI) and phenol adsorption by Dowex 1X8 in the batch study was satisfactorily described by pseudo-second-order model. Thermodynamic study demonstrates the spontaneous and endothermic nature of adsorption process.

Acknowledgement

We would like to thank Tunisian Desalination Association (TDA), TUNISIA for supporting this research.

References

[1] H. Song, Y. Liu, W. Xu, G. Zeng, N. Aibibu, L. Xu, B. Chen, Simultaneous Cr (VI) reduction and phenol degradation in pure cultures of *Pseudomonas aeruginosa* CCTCC AB91095, Bioresour. Technol., 100 (2009) 5079–5084.
[2] S. Golbaz, A.J. Jafari, M. Rafiee, R.R. Kalantary, Separate and simultaneous removal of phenol, chromium, and cyanide from aqueous solution by coagulation/precipitation: mechanisms and theory, Chem. Eng. J., 253 (2014) 251–257.
[3] A. Gupta, C. Balomajumder, Simultaneous adsorption of Cr (VI) and phenol onto tea waste biomass from binary mixture: multicomponent adsorption, thermodynamic and kinetic study, J. Environ. Chem. Eng., 3 (2015) 785–796.
[4] M. Arulkumar, K. Thirumalai, P. Sathishkumar, T. Palvannan, Rapid removal of chromium from aqueous solution using novel prawn shell activated carbon, Chem. Eng. J., 185 (2012) 178–186.
[5] J. Cao, Y. Wu, Y. Jin, P. Yilihan, W. Huang, Response surface methodology approach for optimization of the removal of chromium (VI) by NH_2-MCM-41, J. Taiwan Inst. Chem. Eng., 45 (2014) 860–868.
[6] B. Agarwal, C. Balomajumder, P.K Thakur, Simultaneous co-adsorptive removal of phenol and cyanide from binary solution using granular activated carbon, Chem. Eng. J., 228 (2013) 655–664.
[7] V. Neagu, S. Mikhalovsky, Removal of hexavalent chromium by new quaternized crosslinked poly (4-vinylpyridines), J. Hazard. Mater., 183 (2010) 533–540.
[8] L.M. De Oliveira, L.Q. Ma, J.A. Santos, L.R. Guilherm, Effects of arsenate, chromate, and sulfate on arsenic and chromium uptake and translocation by arsenic hyperaccumulator *Pteris vittata* L. Environ. Pollut., 184 (2014) 187–192.
[9] N. Talreja, D. Kumar, N. Verma, Removal of hexavalent chromium from water using Fe-grown carbon nanofibers containing porous carbon microbeads, J. Water Process Eng., 3 (2014) 34–45.
[10] S. Kumar, M. Zafar, J.K. Prajapati, S. Kumar, S. Kannepalli, Modeling studies on simultaneous adsorption of phenol and resorcinol onto granular activated carbon from simulated aqueous solution, J. Hazard. Mater., 185 (2011) 287–294.
[11] G. Yang, L. Tang, G. Zeng, Y. Cai, J. Tang, Y. Pang, W. Xiong, Simultaneous removal of lead and phenol contamination from water by nitrogen-functionalized magnetic ordered mesoporous carbon, Chem. Eng. J., 259 (2015) 854–864.
[12] E. Pehlivan, S. Cetin, Sorption of Cr (VI) ions on two Lewatit-anion exchange resins and their quantitative determination using UV–visible spectrophotometer, J. Hazard. Mater., 163 (2009) 448–453.
[13] A. Fakhri, Application of response surface methodology to optimize the process variables for fluoride ion removal using maghemite nanoparticles, J. Saudi Chem. Soc., 18 (2014) 340–347.
[14] M. Sabonian, M.A. Behnajady, Artificial neural network modeling of Cr (VI) photocatalytic reduction with TiO_2-P25 nanoparticles using the results obtained from response surface

methodology optimization, Desal. Wat. Treat., 56 (2015) 2906–2916.
[15] J.P. Maran, B. Priya, Comparison of response surface methodology and artificial neural network approach towards efficient ultrasound-assisted biodiesel production from muskmelon oil, Ultrason. Sonochem., 23 (2015) 192–200.
[16] N.G. Turan, B. Mesci, O. Ozgonenel, The use of artificial neural networks (ANN) for modeling of adsorption of Cu (II) from industrial leachate by pumice, Chem. Eng. J., 171 (2011) 1091–1097.
[17] M. Khajeh, M.G. Moghaddam, M. Shakeri, Application of artificial neural network in predicting the extraction yield of essential oils of *Diplotaenia cachrydifolia* by supercritical fluid extraction, J. Supercrit. Fluids, 69 (2012) 91–96.
[18] F. Geyikçi, E. Kılıç, S. Çoruh, S. Elevli, Modelling of lead adsorption from industrial sludge leachate on red mud by using RSM and ANN, Chem. Eng. J., 183 (2012) 53–59.
[19] G.E.P. Box, K.B. Wilson, On the experimental attainment of optimum conditions, Roy. Statist. Soc, Ser. B., 13 (1951) 1–38.
[20] M. Sarkar, D. Santra, Modeling fluoride adsorption on cerium-loaded cellulose bead—response surface methodology, equilibrium, and kinetic studies, Water Air Soil Pollut., 226 (2015) 1–14.
[21] M. Roosta, M. Ghaedi, A. Daneshfar, S. Darafarin, R. Sahraei, M.K. Purkait, Simultaneous ultrasound-assisted removal of sunset yellow and erythrosine by ZnS: Ni nanoparticles loaded on activated carbon: optimization by central composite design, Ultrason. Sonochem., 21 (2014) 1441–1450.
[22] M.B. Hossain, N.P. Brunton, A. Patras, B. Tiwari, C.P.O. Donnell, A.B. Martin-Diana, C.B. Ryan, Optimization of ultrasound assisted extraction of antioxidant compounds from marjoram (*Origanum majorana* L.) using response surface methodology, Ultrason. Sonochem., 19 (2012) 582–590.
[23] A. Asfaram, M. Ghaedi, S. Hajati, A. Goudarzi, A.A. Bazrafshan, Simultaneous ultrasound-assisted ternary adsorption of dyes onto copper-doped zinc sulfide nanoparticles loaded on activated carbon: optimization by response surface methodology, Spectrochim. Acta, Part A, 145 (2015) 203–212.
[24] G. Derringer, R. Suich, Simultaneous optimization of several response variables, J. Qual. Technol., 12 (1980) 214–219.
[25] M. Dutta, J.K. Basu, Application of artificial neural network for prediction of Pb (II) adsorption characteristics, Environ. Sci. Pollut. Res., 20 (2013) 3322–3330.
[26] H. Ebrahimzadeh, N. Tavassoli, O. Sadeghi, M.M. Amini, Optimization of solid-phase extraction using artificial neural networks and response surface methodology in combination with experimental design for determination of gold by atomic absorption spectrometry in industrial wastewater samples, Talanta, 97 (2012) 211–217.
[27] W. Song, B. Gao, X. Xu, L. Xing, S. Han, P. Duan, R. Jia, Adsorption–desorption behavior of magnetic amine/Fe_3O_4 functionalized biopolymer resin towards anionic dyes from wastewater, Bioresour. Technol., 210 (2016) 123–130.
[28] Y. Zhou, Q. Jin, T. Zhu, Y. Akama, Adsorption of chromium (VI) from aqueous solutions by cellulose modified with β-CD and quaternary ammonium groups, J. Hazard. Mater., 187 (2011) 303–310.
[29] F. Nekouei, S. Nekouei, I. Tyagi, V.K. Gupta, Kinetic, thermodynamic and isotherm studies for acid blue 129 removal from liquids using copper oxide nanoparticle-modified activated carbon as a novel adsorbent, J. Mol. Liq., 201 (2015) 124–133.
[30] S. Sugashini, K.M.M.S. Begum, Optimization using central composite design (CCD) for the biosorption of Cr(VI) ions by cross linked chitosan carbonized rice husk (CCACR), Clean Technol. Environ. Policy, 15 (2012) 293–302.
[31] K. Abburi, Adsorption of phenol and p-chlorophenol from their single and bisolute aqueous solutions on Amberlite XAD-16 resin, J. Hazard. Mater., 105 (2003) 143–156.
[32] S. Mondal, K. Aikat, G. Halder, Optimization of ranitidine hydrochloride removal from simulated pharmaceutical waste by activated charcoal from mung bean husk using response surface methodology and artificial neural network, Desal. Wat. Treat., 57 (2016) 18366–18378.
[33] M.R. Awual, M.A. Shenashen, T. Yaita, H. Shiwaku, A. Jyo, Efficient arsenic (V) removal from water by ligand exchange fibrous adsorbent, Water Res., 46 (2012) 5541–5550.
[34] A. Gundogdu, C. uran, H. Basri Senturk, M. Soylak, D. Ozdes, H. Serencam, M. Imamoglu, Adsorption of phenol from aqueous solution on a low-cost activated carbon produced from tea industry waste: equilibrium, kinetic, and thermodynamic study, J. Chem. Eng. Data, 57 (2012) 2733–2743.
[35] C. Ling, F.-Q. Liu, C. Long, T.-P. Chen, Q.Y. Wu, A.M. Li, Synergic removal and sequential recovery of acid black 1 and copper (II) with hyper-crosslinked resin and inside mechanisms, Chem. Eng. J., 236 (2014) 323–331.
[36] J.C. Lazo-Cannata, A. Nieto-Márquez, A. Jacoby, A.L. Paredes-Doig, A. Romero, M.R. Sun-Kou, J.L. Valverde, Adsorption of phenol and nitrophenols by carbon nanospheres: effect of pH and ionic strength, Sep. Purif. Technol., 80 (2011) 217–224.
[37] M.H. Uddin, B. Nanzai, K. Okitsu, Effects of Na_2SO_4 or NaCl on sonochemical degradation of phenolic compounds in an aqueous solution under Ar: positive and negative effects induced by the presence of salts, Ultrason. Sonochem., 28 (2016) 144–149.